ELSEVIER

Shock wave induced damage in kidney tissue

K. Weinberg [a,*], M. Ortiz [b]

[a] *Mechanical Institute, MS2, Technical University of Berlin, Einsteinufer 5, D-10587 Berlin, Germany*
[b] *Graduate Aeronautical Laboratories, California Institute of Technology, Pasadena, CA 91125, USA*

Abstract

In a common medical procedure known as shock-wave lithotripsy hypersonic waves are generated and focused at the kidney stone. These shock waves are thought to fragment the stone but also lead to injuries of the kidney tissue. To predict and estimate this damage we develop here a mechanical model for the response of soft tissue to the exposure of shock waves.

The material model combines shear induced finite plasticity with irreversible volumetric expansion as induced, e.g., by cavitating bubbles. Dynamic effects like micro-inertia and rate sensitivity are included. The time-discretized porous-viscoplastic constitutive updates are described in a fully variational manner. A finite element analysis localizes the damage in the human kidney in good agreement to clinical and experimental studies.
© 2004 Elsevier B.V. All rights reserved.

1. Introduction

In extracorporeal shock-wave lithotripsy (SWL)—a non-invasive procedure to comminute kidney stones—a number of high intensity sound waves (shock waves) are generated outside the patient and focused on the stone within the kidney. A compressive wave with a typical peak pressure of 30–80 MPa (see Fig. 1a), induces cracks and, by internal reflection, spallation in the stone. Unfortunately, the focused wave front also causes shearing along its way in the kidney tissue which may be responsible for severe kidney injuries. Moreover, the compressive front is followed by a "tension tail", i.e., a negative pressure up to 10 MPa. In this way bubble cavitation is induced which is thought to assist in stone comminution, cf. [6]. Bubbles nucleate, expand up to several micrometer in size and finally collapse emitting "micro-jets". This yields typical pitting pattern on the surface of the stone, see Fig. 1b. During bubble expansion the surrounding vessels and capillaries dilate and

---

* Corresponding author.
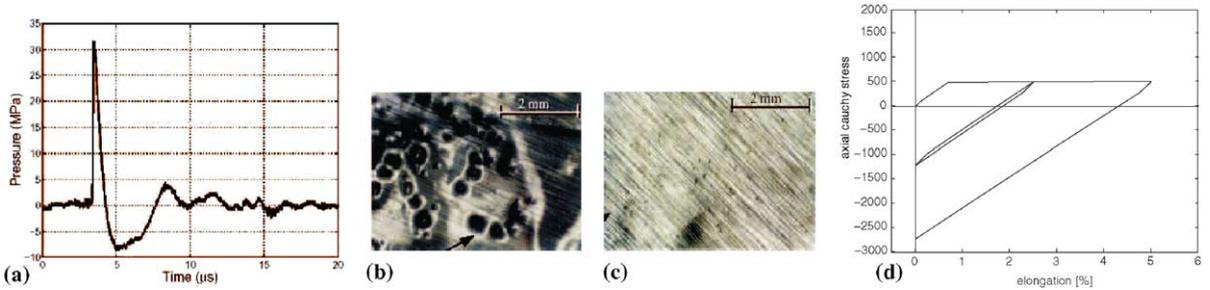*E-mail address:* kerstin.weinberg@tu-berlin.de (K. Weinberg).

Fig. 1. Shock wave, experimentally observed effect of cavitation in tension (pitting) and pressure (no effect), cf. [2], and stresses computed in two cycles of a uniaxial strain test: (a) typical SWL-pressure wave; (b) pitting; (c) over-pressure and (d) Cauchy stress vs. elongation.

may rupture. This mechanism causes irreversible changes of the kidney tissue material due to hydrostatic tension.

With a view to simulating the SWL-process by finite element analysis we provide in this paper a phenomenological material model for kidney tissue. This model accounts for irreversible damage due to shearing as well as for local damage caused by hydrostatic tension. Kidney tissue is not well investigated, therefore one goal of our modelling was to keep the set of necessary material data as small as possible. Moreover we do not analyze the micro-histological changes in detail, this would require an other scale of modelling. Instead we summarize the morphological lesions like hemorrhage, rupture of small arteries and tearing of peri-tubular capillaries, as damage in the sense of irreversible deformations to approach numerically the high-speed process of SWL.

2. The model

The equilibrium response of the solids considered in this work is characterized by a free-energy density per unit undeformed volume of the form

$$A = A(\boldsymbol{F}, T, \boldsymbol{F}^{\mathrm{p}}, \varepsilon^{\mathrm{p}}, \theta^{\mathrm{p}}), \tag{1}$$

where $\boldsymbol{F}$ is the deformation gradient, T is the absolute temperature, ε^{p} and ϑ^{p} are internal variables, $\boldsymbol{F}^{\mathrm{p}}$ is the plastic deformation, and $\boldsymbol{F}^{\mathrm{e}} = \boldsymbol{F}\boldsymbol{F}^{p-1}$ is the elastic deformation. The underlying assumption is that (1) attains a minimum at $\boldsymbol{F}^{\mathrm{e}} =$

$\boldsymbol{R}^{\mathrm{e}} \in \mathrm{SO}(3)$, so that the material is stress-free whenever $\boldsymbol{F} = \boldsymbol{R}^{\mathrm{e}}\boldsymbol{F}^{\mathrm{p}}$.

The plastic deformation rate is assumed to obey the flow rule:

$$\dot{\boldsymbol{F}}^{\mathrm{p}}\boldsymbol{F}^{\mathrm{p}-1} = \dot{\varepsilon}^{\mathrm{p}}\boldsymbol{M} + \dot{\vartheta}^{\mathrm{p}}\boldsymbol{N}, \tag{2}$$

where $\dot{\varepsilon}^{\mathrm{p}}$ and $\dot{\vartheta}^{\mathrm{p}}$ are scalar variables accounting for irreversible (plastic) deformation subjected to the constraints

$$\dot{\varepsilon}^{\mathrm{p}} \geqslant 0 \quad \text{and} \quad \dot{\vartheta}^{\mathrm{p}} \geqslant 0. \tag{3}$$

The tensors $\boldsymbol{M}$ and $\boldsymbol{N}$ set the direction of the deviatoric and volumetric plastic deformation rates, respectively. Tensor $\boldsymbol{M}$ is assumed to be trace-free and normalized

$$|\boldsymbol{M}|^2 = \frac{3}{2} \quad \text{and} \quad \mathrm{tr}(\boldsymbol{M}) = 0, \tag{4}$$

whereas the tensor $\boldsymbol{N}$ is allowed to take one of two values,

$$\boldsymbol{N} = \pm\frac{1}{3}\boldsymbol{I}, \tag{5}$$

with the plus sign corresponding to volumetric expansion and the minus sign to compression. The tensors $\boldsymbol{M}$ and $\boldsymbol{N}$ are otherwise unknown and are to be determined as part of the solution. The constraints (4) and (5) may be regarded as defining the assumed kinematics of plastic deformation.

It is useful to note that for purely volumetric deformations the flow rule (2) reduces to

$$\frac{\mathrm{d}}{\mathrm{d}t}\log J^{\mathrm{p}} = \mathrm{tr}(\boldsymbol{N})\dot{\vartheta}^{\mathrm{p}} = \pm\dot{\vartheta}^{\mathrm{p}}. \tag{6}$$

From (6) we find upon integration

$$\vartheta^{\mathrm{p}}(t) = \vartheta^{\mathrm{p}}(0) + \int_0^t \left|\frac{\mathrm{d}}{\mathrm{d}\xi}\log J^{\mathrm{p}}(\xi)\right|\mathrm{d}\xi \tag{7}$$

i.e., the variable ϑ^{p} is a measure of the accumulated irreversible volumetric deformation. Evidently, ϑ^{p} and $\log J^{\mathrm{p}}$ coincide up to a constant for monotonic expansion as given here, but the distinction between the two variables becomes important for arbitrary loading programs.

In order to formulate a complete set of constitutive relations, the free-energy density and appropriate rate equations for the internal variables ε^{p} and ϑ^{p} must be specified. Using a relatively simple dilute distribution of (empty) spherical bubbles we link the mechanism of bubble expansion causing irreversible damage to the macroscopic material parameter. To this end we consider a material of volume V and determine the local volume fraction of bubbles in the deformed configuration as

$$f = N\frac{V_0}{V}\frac{4\pi a^3}{3}, \tag{8}$$

where here and subsequently the subindex 0 designates fields defined on the reference configuration; a is current average bubble radius and N is the referential bubble density, i.e., the number of bubbles per unit volume. The volumes V_0 and V are related through $V = JV_0$ where

$$J \equiv \det \boldsymbol{F} = \det(\boldsymbol{F}^{\mathrm{e}}\boldsymbol{F}^{\mathrm{p}}) = \det \boldsymbol{F}^{\mathrm{e}} \det \boldsymbol{F}^{\mathrm{p}} \equiv J^{\mathrm{e}}J^{\mathrm{p}} \tag{9}$$

is the local Jacobian of the deformation and J^{e} and J^{p} are the corresponding elastic and plastic components. Using these relations we have

$$J^{\mathrm{p}} = V(J^{\mathrm{e}}V_0)^{-1} = (1 - f_0)/(1 - f), \tag{10}$$

i.e., J^{p} is the ratio of the volumes of infinitesimal material neighborhoods in the intermediate, or plastically-deformed, configuration and in the reference configuration. This allows f to be computed from J^{p} and, using (8), (10) may be recast in terms of the bubble radius, with the result

$$J^{\mathrm{p}} = 1 - f_0 + \frac{V}{J^{\mathrm{e}}V_0}f = 1 - N\frac{4\pi a_0^3}{3} + N\frac{4\pi a^3}{3J^{\mathrm{e}}}. \tag{11}$$

It is worth to note that the volumetric plastic deformation depends on the "rigid-plastic" radius, $\bar{a} = J^{\mathrm{e}-1/3}a$, representing a cavity size in the intermediate configuration. In terms of $\bar{a}$ (11) simplifies to

$$J^{\mathrm{p}} = 1 + \frac{4\pi}{3}N(\bar{a}^3 - a_0^3) \quad \text{and}$$

$$\bar{a} = \left[\frac{3}{4\pi}\frac{1}{N}(J^{\mathrm{p}} - 1) + a_0^3\right]^{1/3} \tag{12}$$

which allows $\bar{a}$ to be computed from J^{p}. The distinction between a and $\bar{a}$ becomes important in the presence of volumetric elastic deformations but may easily be neglected here.

The free-energy density (1) is assumed to decompose additively into elastic and stored plastic energy densities, $W(\boldsymbol{F}^{\mathrm{e}}, T)$ and $W^{\mathrm{p}}(T, \varepsilon^{\mathrm{p}}, \theta^{\mathrm{p}})$, respectively. Due to material-frame indifference, W^{e} can only depend on $\boldsymbol{F}^{\mathrm{e}}$ through the corresponding elastic right-Cauchy Green deformation tensor

$$\boldsymbol{C}^{\mathrm{e}} = \boldsymbol{F}^{\mathrm{eT}}\boldsymbol{F}^{\mathrm{e}} = \boldsymbol{F}^{\mathrm{p-T}}\boldsymbol{C}\,\boldsymbol{F}^{\mathrm{p-1}}. \tag{13}$$

Without loss of generality, the elastic strain-energy density may alternatively be expressed in terms of the logarithmic elastic strain $\epsilon^{\mathrm{e}} = \frac{1}{2}\log(\boldsymbol{C}^{\mathrm{e}})$, i.e., $W^{\mathrm{e}} = W^{\mathrm{e}}(\boldsymbol{C}^{\mathrm{e}}, T) = W^{\mathrm{e}}(\epsilon^{\mathrm{e}}, T)$. We denote by $\boldsymbol{\sigma}$ the stress conjugate to ϵ^{e}, namely,

$$\boldsymbol{\sigma} = \frac{\partial W^{\mathrm{e}}}{\partial \epsilon^{\mathrm{e}}}(\epsilon^{\mathrm{e}}, T). \tag{14}$$

The first Piola–Kirchhoff stress tensor $\boldsymbol{P}$ follows from Coleman's relations as $\boldsymbol{P} = \partial A/\partial \boldsymbol{F}$ and can be evaluated by

$$\boldsymbol{P} = \frac{\partial W^{\mathrm{e}}}{\partial \boldsymbol{F}} = \frac{\partial W^{\mathrm{e}}}{\partial \epsilon^{\mathrm{e}}} \cdot \frac{\partial \epsilon^{\mathrm{e}}}{\partial \boldsymbol{C}} \cdot \frac{\partial \boldsymbol{C}}{\partial \boldsymbol{F}}. \tag{15}$$

We note that, whereas the dependence of W^{e} and, correspondingly, of $\boldsymbol{\sigma}$ on ϵ^{e} is material-specific, the transformations required to convert $\boldsymbol{\sigma}$ to $\boldsymbol{P}$ are material-independent. Further stress contributions may result from viscosity.

In our calculations we specifically take W^{e} to be quadratic and isotropic in the logarithmic elastic strains and consider the process to be isotherm, i.e.,

$$W^{\mathrm{e}} = W^{\mathrm{e}}(\boldsymbol{F}^{\mathrm{e}}) = \frac{\kappa}{2}[\log J^{\mathrm{e}}]^2 + \frac{\mu}{4}\|\mathrm{dev}(\epsilon^{\mathrm{e}})\|^2, \tag{16}$$

where κ and μ are a reference bulk and shear modulus. The stress relations follow from (16) by an application of (15). In particular, the pressure in the tissue is linear in the elastic logarithmic volumetric strain.

A simple stored plastic energy function may be formulated by an additive decomposition into volumetric and deviatoric components. The latter, solely a function of the effective deviatoric plastic strain ε^p, follows a conventional power-law of hardening

$$W^p(\varepsilon^p) = \frac{n\sigma_0\varepsilon_0^p}{n+1}\left[\left(1+\frac{\varepsilon^p}{\varepsilon_0^p}\right)^{(n+1)/n} - 1\right], \qquad (17)$$

where σ_0 is the yield stress, n is the hardening exponent and ε_0^p is a reference parameter. The volumetric part of the dissipated energy function is attributed directly to the bubble growth. In the dilute limit, the total energy stored by expanded bubbles is the sum of the energy dissipated by each individual bubble. For empty spherical cavities (voids) in a power-law hardening material the stored energy has been determined by Ortiz and Molinari [4]. This equals the plastic work of deformation attendant to the expansion of bubbles. Following these considerations and referring it to the unit volume by the Jacobian J^p lead to the stored energy function

$$W^p(\varepsilon^p, \vartheta^p) = W^p(\varepsilon^p) + \frac{n\sigma_0\varepsilon_0^p}{(n+1)}N\frac{4\pi\bar{a}^3}{3}\left(\frac{2}{3\varepsilon_0^p}\right)^{(n+1)/n}$$
$$\times \int_1^\infty \left\{\log\frac{x}{x-1+[1+(e^{\vartheta^p}-1)/f_0]^{-1}}\right\}^{(n+1)/n} dx. \qquad (18)$$

Aside of conventional Newtonian viscosity we consider two types of rate effects: rate sensitivity in the plastic deformations and micro-inertia due to rapidly expanding bubbles. To ensure a variational structure we postulate the existence of a dual kinetic potential $\psi^*(\dot{\varepsilon}^p, \dot{\vartheta}^p, J^p)$ such that the thermodynamic forces conjugate to $\dot{\varepsilon}^p$ and $\dot{\vartheta}^p$ may be derived from ψ^*. The modelling of rate sensitivity follows analogous to the plastic work function, cf. [7]. Micro-inertia as a dissipative energy term is a somewhat non-standard feature of the present model, it renders the equations of motion for the growth of the bubbles of second order

in time. In a dilute model the total micro-inertia attendant to the growth of the bubble ensemble is the sum of the kinetic energies due to the expansion of each individual bubble and can be computed readily with the result

$$K(\bar{a}, \dot{\bar{a}}) = 2\pi N\varrho_0\bar{a}^3\dot{\bar{a}}^2, \qquad (19)$$

where ϱ_0 is the mass density per unit volume. In order to formulate updates possessing a variational structure, the time-discretization of the equations of motion must itself possess an incremental variational structure. By a change of variables function (19) may be transformed adequately, cf. [7].

For implementation we start by discretizing the flow rule in time using an exponential mapping technique with the result

$$\boldsymbol{F}_{n+1}^p = \exp(\Delta\varepsilon^p\boldsymbol{M} + \Delta\vartheta^p\boldsymbol{N})\boldsymbol{F}_n^p. \qquad (20)$$

Clearly, the update (20) is consistent with the flow rule (2) by virtue of the identity

$$\left\{\frac{d}{dt}\exp[t(\dot{\varepsilon}^p\boldsymbol{M} + \dot{\vartheta}^p\boldsymbol{N})]\right\}_{t=0^+} = \dot{\varepsilon}^p\boldsymbol{M} + \dot{\vartheta}^p\boldsymbol{N}. \qquad (21)$$

We update the internal state variables, ε_{n+1}^p and ϑ_{n+1}^p, and simultaneously determine the incremental direction of plastic flow, $\boldsymbol{M}$ and $\boldsymbol{N}$, for the time step by recourse to the variational formulation of Ortiz and Stainier [5]. To this end, we introduce in every time interval $\Delta t = t_{n+1} - t_n$ the incremental objective function

$$f_n(\boldsymbol{F}_{n+1}, \varepsilon_{n+1}^p, \vartheta_{n+1}^p, \boldsymbol{M}, \boldsymbol{N})$$
$$= W^e(\boldsymbol{C}_{n+1}^e) + W^p(\varepsilon_{n+1}^p, \vartheta_{n+1}^p, J_{n+1}^p)$$
$$+ K(\vartheta_{n+1}^p, \dot{\vartheta}_{n+1}^p, J_{n+1}^p)$$
$$+ \Delta t\psi^*(\triangle\varepsilon^p/\triangle t, \triangle\vartheta^p/\triangle t, J_{n+1}^p). \qquad (22)$$

We emphasize that this function includes the free energy of the material, as well as the stored energy, the micro-kinetic energy and the dual kinetic potential. These contributions compete in energetic terms, and the optimal internal process is that one which minimizes the function f_n. This may be expressed in variational form as

$$W_n(\boldsymbol{F}_{n+1}) = \min_{\varepsilon_{n+1}^p, \vartheta_{n+1}^p, \boldsymbol{M}, \boldsymbol{N}} f_n(\boldsymbol{F}_{n+1}, \varepsilon_{n+1}^p, \vartheta_{n+1}^p, \boldsymbol{M}, \boldsymbol{N})$$
$$\qquad (23)$$

subject to the constraints (4) and (5). Note that (23) acts as a potential for the stress–strain relations, the tangent moduli are consequently symmetric.

Fig. 1d shows the computed axial Cauchy stress in a uniaxial bar subjected to cyclic elongation. By constraining (5) to a positive sign, we only allow for irreversibility in tension. This is motivated by experimental observations [2].

3. Numerical simulation

For finite element analysis we build an anatomical correct mesh of a human kidney using geometrical data from image processing (Fig. 2). The kidney is modelled without a stone. This approach is backed by experimental studies showing that injuries are caused by SWL treatment and hardly influenced by stone fragmentation [1]. For a first
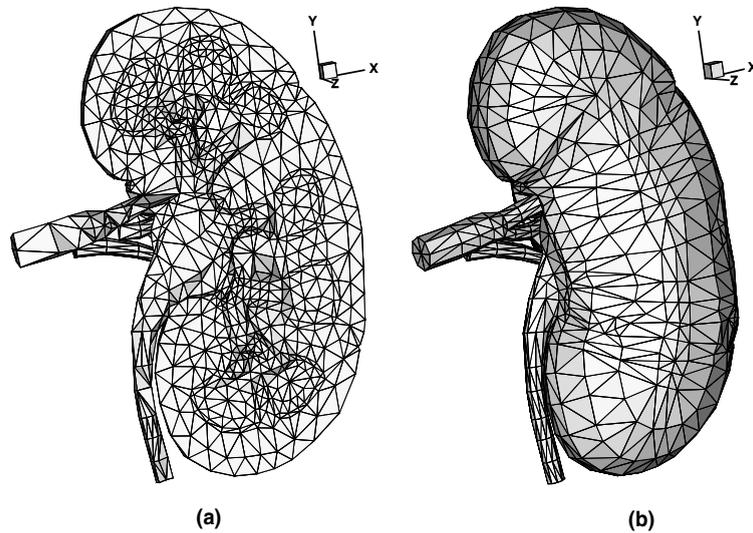

Fig. 2. Anatomically correct finite element mesh of the kidney. (a) Meridional section and (b) full model.
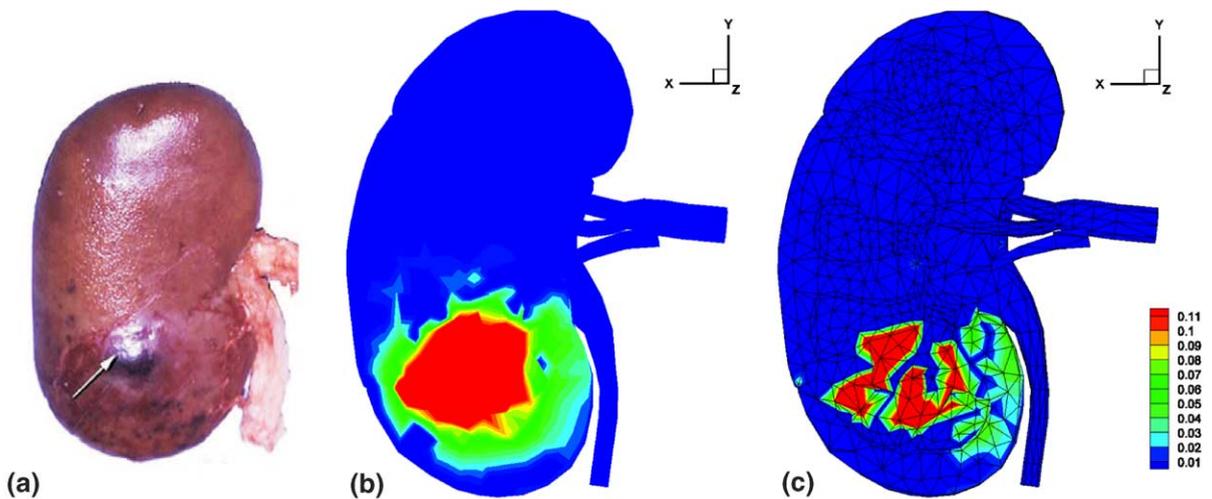

Fig. 3. Typical bruising observed in an animal experiment from [1] and the computed field of irreversible volumetric expansion: (a) pig kidney, (b) exterior view and (c) meridional section.

computation we only distinguish regions of functional (sensitive) kidney tissue and non-functional tissue (as, e.g., the ureter and main blood vessels), modelled with the presented material and a nonlinear elastic material law, respectively. Material parameters available from experiments are homogenized for "the kidney" disregarding the interior structure, (cf. [1,3,8] and references therein). We use here: $E = 0.1$ MPa, $\kappa = 250$ MPa, $\sigma_0 = 80$ Pa, exponents $m = n = 10$, $\rho = 1050$ kg/m^3 and viscosity $\eta = 0.005$ Pa s.

The unsupported kidney was subjected to a 1 μs pressure wave modelled as distributed force on the boundary and then released. For time integration we apply an explicit Newmark scheme over a period of 100 μs [7].

Common evidence of shock wave induced morphological lesions are kidney enlargement, bruising and hemorrhage in the pre-focal area, see the photograph of a SWL subjected pig kidney in Fig. 3. The location of injuries correlates to the area of peak negative pressure and greatest cavitation [6]. This effect is captured by our kidney model. Fig. 3 shows the computed field of irreversible volumetric dilatation on the boundary and in the focal area (meridional section). The irreversible volumetric expansion is induced by hydrostatic tension following the shock front and additionally caused by reflection of the applied pressure wave.

We observe an encouraging agreement of localized damaged. Further research is ongoing to study the influence of the surrounding body tissue and the effect of varying material data.

References

[1] R.O. Cleveland, D.A. Lifshitz, B.A. Connors, A.P. Evan, L.R. Willis, L.A. Crum, In vivo pressure measurements of lithotripsy shock waves in pigs, Ultrasound Med. Biol. 24 (2) (1998) 293–306.

[2] M. Lokhandwalla, Damage Mechanisms in Shock Wave Lithotripsy, Ph.D. Thesis, California Institute of Technology, 2001.

[3] S. Nasseri, L.E. Bilston, N. Phan-Thien, Viscoelastic properties of pig kidney in shear, experimental results and modelling, Rheol. Acta 41 (2002) 180–192.

[4] M. Ortiz, A. Molinari, Effect of strain hardening and rate sensitivity on the dynamic growth of a void in a plastic material, Trans. ASME 59 (1992) 48–53.

[5] M. Ortiz, L. Stainier, The variational formulation of viscoplastic constitutive updates, CMAME 171 (3–4) (1999) 419–444.

[6] M. Tanguay, T. Colonius, Numerical investigation of bubble cloud dynamics in SWL, in: Proc. of FEDSM'02, ASME, Montreal, Canada, 2002.

[7] K. Weinberg, A variational formulation for porous plasticity, preprint TU, Berlin, 2004.

[8] L.R. Willis, A.P. Evan, B.A. Connors, P. Blomgren, N.S. Fineberg, J.F. Lingeman, Relationship between kidney size, renal injury, and renal impairment induced by SWL, J. Am. Soc. Nephrol. 10 (1999) 1753–1762.